Detection of Ore Type in Drilling Cores Using Deep Learning[1]

Pouya Nobahar and Yashar Pourrahimian
Mining Optimization Laboratory (MOL)
University of Alberta, Edmonton, Canada

ABSTRACT

Some of the most common mining processes include mine design and mineral reserve evaluation using data from exploratory boreholes. However, preparing core samples and conducting chemical and physical tests on them costs time and money, slowing down the modelling process. This paper presents a novel deep learning (DL) algorithm to recognize the types of kaolin samples. For this purpose, a dataset of drilled cores' images and their relative types, which is examined using chemical and physical analyses, is used. Two eight-layer convolutional neural network (CNN) topologies (A and B) based on individual features are presented. The results show that Model A is more efficient with 91 percent accuracy than Model B with 84 percent accuracy. Furthermore, the exactness of recognizing the model according to four criteria, including accuracy, precision, recall, and F1-score, is equal to 90%, 92%, 92%, and 90%, respectively, which are acceptable accuracies to identify the type of samples when using this approach on six different types of kaolin.

1. Introduction

The use of exploratory borehole data in mine design and evaluation of mineral reserves is one of the essential stages of mining operations, which significantly affects the project's viability. Chemical and physical tests are performed on drilled cores, and the quantity of elements in the samples is estimated using this procedure. These analyses are either employed continuously (grades) or as classifications. Preparing core samples and conducting chemical and physical tests on them cost time and money, slowing down the modelling process. But, in order to obtain a realistic approach, standard methodologies have lately been upgraded by combining industrial and computer science. As an illustration, texture characteristics were derived from real rock photos used in bedrock research by Lepisto et al. (2005), using various scales, applied a Gaussian bandpass filter to the image's colour channels in RGB (red, green, blue) and HIS (hue, saturation, intensity) colour spaces. The results suggest that combining different colour channels improves categorization accuracy substantially. In the same year, Singh and Rao (2005) proposed a new method for classifying ores in ferromanganese metallurgical plants. The ore particles' visual texture (Mn, Fe, and Al_2O_3 rich) and a radial basis neural network were used to develop their approach. The results demonstrate that the technique may be used to construct an expert system for online ore quality monitoring, which can be used to manage ore blending in feed ore circuits as well as separate gangue minerals present in feed ores. Baykan and Yilmaz (2010) used colour spaces and artificial neural networks (AAN) to investigate mineral identification. Their proposed network

[1] A version of this paper has been submitted to the journal of Computers and Geosecinces

ISBN: 978-1-55195-486-8

classifies five different minerals (quartz, muscovite, biotite, chlorite, and opaque) using six different input parameters. The network performed well with previously encountered mineral samples, with success rates ranging from 81 to 98%. Chatterjee et al. (2010) used a neural network model as a mapping function for ore quality monitoring and grade prediction. The findings showed that this approach might be utilized to monitor ore grade at the mine level in a controlled setting. Khorram et al. (2012) created an ore grade prediction model using image processing and pattern recognition approaches. The concept accurately predicted the proportion of chemical constituents of samples taken from the same mine. Keyvani and Strom (2013) created a completely automated image processing script for analyzing massive datasets of photographed flocs in mud suspensions in dilute turbulent suspensions. Liu et al. (2013) developed software called "Crack Image Analysis System" (CIAS) to evaluate the geometric features of crack networks. Various geometric characteristics, such as node-and-crack-numbers, cold area, clod perimeter, crack area, thickness, length, and direction, can be determined automatically using this program. In addition, Gan and Scholz (2013) published a technique for measuring and precisely extracting lamina characteristics from sedimentary core pictures. Patel and Chatterjee (2016) proposed a computer vision-based rock-type classification system for quick and accurate detection even without human involvement. A probabilistic neural network (PNN) with color histogram data as feed was utilized to construct a laboratory-scale vision-based model. The cumulative miss-classification loss for this approach was less than 6%. Chauhan et al. (2016) looked at how to segment X-ray digital micro tomography rock pictures and predict pore spacing and pore size sizes using unsupervised, supervised, and ensemble clustering algorithms. Maiti et al. (2017) created a mass framework that translates the image-based size distribution to a mass-wise distribution, allowing it to be compared to mechanical filtration data. For mass rebuilding from 2D pictures of particle aggregates, the idea of weight/particle ratio was presented. Ramil et al. (2018) improved a backpropagation ANN to quickly and precisely recognize formation minerals in granites using RGB images. Their research led to the identification of the forming minerals for three independent granitic kinds with good accuracy. Maitre et al. (2019) proposed a novel methodology for automating mineral grain identification from numerically pictures generated with a basic microscope. This study generates super-pixels using basic linear iterative grouping segmentation, and almost all of them permit separating sand grains, which is impossible with traditional segmentation approaches. Finally, Ran et al. (2019) reported an efficient measure for recognizing rock kinds in the field using a CNN model and image analysis. With excellent prediction performance, the suggested method can identify six common rock kinds. Ouanan and El Hassan (2019) suggested a real-time froth image processing method in mineral processing. Finally, they suggested several future directions, such as data analysis and building an exploration tool based on image processing (IP) and machine learning (ML) algorithms by analyzing geoscience datasets using cloud computing technology to discover target locations with significant development. Safari et al. (2021) presented an image processing approach for analyzing pore and grain size variations in porous geological rocks using X-ray microcomputed tomography and scanning electron microscopy (SEM) images. Also, Liu et al. (2021) created four CNNs algorithms having varying depths and topology for multi coal and multi class image analysis. Their study objects were anthracite, gas coal, and coking coal, and a widespread CNNs model was presented for multi-coal and multi-class sorting.

Above mentioned studies required some laboratory devices and could not identify rock types accurately in a short time. Also, none of them can classify sub-classes of a unique mineral.

By using deep learning (DL) and images related to kaolin types, a model with a fast execution speed, low cost, and high accuracy is presented in this paper to classify the various types of kaolin

samples instead of using chemical and physical analyses. Figure 1 shows two methods of operational flowcharts.

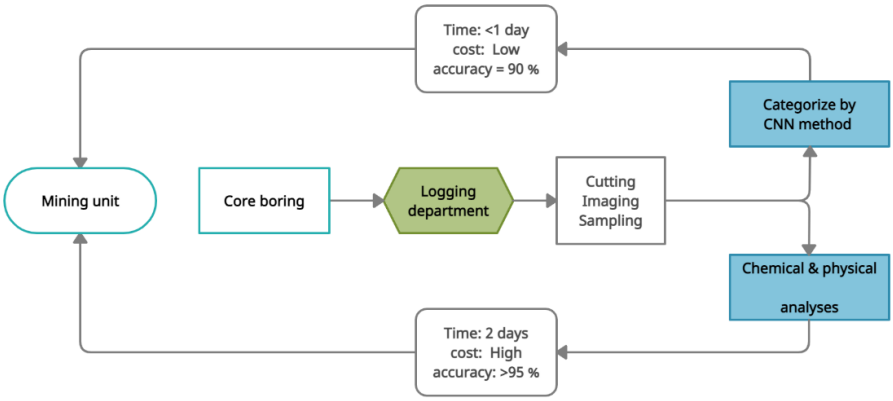

Figure 1. Flow charts of two operational ways.

2. Methodology

ML technologies are progressively adopted in most industries to improve value and solve problems. This technology is based on algorithms that learn how to make predictions based on example inputs. Some of these algorithms allow predictions to be made from images. These DL algorithms are called CNN and can be used for tasks such as classification, object identification, text categorization, and helping individuals. They have been used successfully for numerous applications, including for self-driving cars. The following sections explain different steps of the research.

2.1. Images Acquisition

More than 1000 images of drilled cores were captured in equal conditions with a vertical angle and steady light at a distance of 10 centimeters to generate a data set that is used in the learning and evaluation processes. All images were examined, and 610 high-quality images with a resolution of 666×500 pixels were selected for processing.

2.2. Sample Preparation

Since kaolin is divided into different categories, samples from drilled cores are taken at two-meter intervals. Drilled cores are pre-logged, and intervals are separated based on core characteristics in the logging department to complete this stage. After that, the cores are separated and divided into two parts, which are gathered in a plastic bag. Finally, these bags, which include a unique code that the mining department recognizes, are delivered to a laboratory for analysis.

2.3. Sample Chemical and Physical Analyses

Minerals like kaolin are classified based on the number of impurities, unwanted components and physical characteristics. As a result, five critical properties of samples, including the percentage of Fe_2O_3, Al_2O_3, and CaO as chemical variables, and the percentage of whiteness and the module of ruptures (Kg_f/cm^2) as physical factors are assessed.

2.4. Assumptions

It is assumed that each image has the same characteristics as the other portions of the sample, and the content of the images is extended to all parts at two-meter intervals. In other words, if drilled cores are cut at any angle and depth, all slices will have the same features. 2D samples (images), also reveal properties of the entire interval.

2.5. Deep Learning (DL) and Convolutional Neural Network (CNN)

DL is a subfield of ML that enables computers to learn from past experiences and comprehend their surroundings via layered structures. DL is built on adaptive, durable, and scalable ANNs, making it ideal for large and complex ML challenges like image categorization (Géron, 2017). On the other hand, CNN is a sort of ANN designed to deal with data with a known, grid-like structure, such as image data. Fu and Aldrich (2020) comprehensively reviewed DL in mining and mineral processing operations. Their research reveals that CNNs have already seen the greatest employment far by a considerable margin. Figure 2 shows how several DL algorithms are used in mining. Convolutional neural networks (CNNs), long short-term memory recurrent networks (LSTMs), deep belief networks (DBNs), and deep reinforcement learning (DRL) are examples of such techniques .

To create its network, CNN uses a mathematical method known as convolution, a form of linear operation (Géron, 2017). Tensor-Flow, an end-to-end open-source ML framework, can be used to implement CNN. Also, Keras is a Python-based high-level neural network API that is used with Tensor-Flow. This paper uses these platforms to create models, networks, and executions.

Recursive neural networks (RvNNs), recurrent neural networks (RNNs), and convolutional neural networks (CNNs) are the most well-known varieties of DL networks. RvNN can categorize data and predict the future in a hierarchical framework using compositional vectors (Alzubaidi et al., 2021). In an RNN, sequencing data is used in the network. This property is essential to a variety of applications because the embedded structure in the data sets is essential (Gu et al., 2018). CNN is the most well-known and widely used method in the DL. The fundamental benefit of CNN over its predecessors is that it automatically detects significant elements without human intervention (Socher et al., 2013). CNNs have been widely used in a variety of domains, including computer vision (Fang et al., 2020), voice recognition (Palaz et al., 2019), and face recognition (Li et al., 2020).

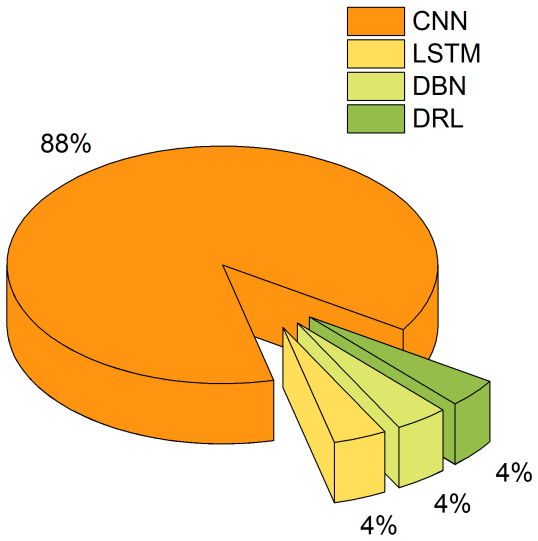

Figure 2. Application of DL algorithms in mining [19].

The benefits of using CNNs over other traditional neural networks in the computer vision environment are (i) the weight sharing feature, which reduces the number of trainable network parameters and, in turn, helps the network to enhance generalization and avoid overfitting, (ii) concurrently learning the feature extraction layers and the classification layer causes the model output to be both highly organized and highly reliant on the extracted features, and (iii) large-scale network implementation, which is much easier with CNN than with other neural networks. Additionally, CNNs have several individual layers described in detail below (Gu et al., 2018).

2.5.1. Convolutional Layer

The convolutional layer is by far the most critical feature in CNN design. It is made up of a number of convolutional filters. The output feature map is generated by convolving the input picture by these filters, which are reflected as N-dimensional attributes.

2.5.2. Pooling Layer

The pooling layer's primary function is to subsample the image data. The convolutional procedures are used to create a similar mapping. In other respects, this method reduces the size of huge input data in order to construct smaller feature maps. At the same time, it keeps the majority of the important data (or characteristics) throughout any stage of the pooling process.

2.5.3. Activation Function

The primary purpose of all forms of activation in all neural networks is to map the extracted features (non-linearity). The adjusted computation of the neuron input and its bias is used to compute the input value. This implies that the activation function creates the clear determination to select whether or not to activate a neuron in response to a particular input.

2.5.4. Fully Connected Layer

This layer is usually found near the conclusion of each CNN architecture. The so-called Fully Connected (FC) technique connects each neuron in this layer to all neurons in the preceding layer. As a CNN classification, it is used. It uses the same fundamental mechanism as a traditional multiple-layer perceptron neural network as a feed-forward ANN. The FC layer receives its input

from the previous pooling or convolutional layer. This vector is made from the feature maps when they have been flattened.

2.5.5. Loss Functions

The output layer, the final layer of the CNN architecture, is used to produce the final categorization. The anticipated error produced throughout the training samples in the CNN model is calculated using several loss functions in the output layer. This inaccuracy reveals the disparity in both the observed and forecast production. The CNN learning process will then be used to improve that as well.

3. Case Study

Zenouz kaolin mine is located near Zenouz city, approximately 15 km north of Marand city of East Azerbaijan, Iran. Figure 3 illustrates the location of the Zenouz kaolin mine.

Figure 3. Location of Zenouz kaolin mine.

Core boring is done to prepare drilling cores in this mine, which are then utilized to design the mine, estimate the ore reserves, and finally, mine planning based on this data. Drilled cores are transferred to the logging department, which records data and prepares samples. Figure 4 shows an example of a drilled core's stocking box containing information from a borehole. The cores are cut and separated into two portions in the logging department, as shown in Figure 5. The first part is stored in the box as an archive, while the second part is sent to the laboratory in two-meter intervals for physical and chemical analyses and kaolin type determination. Table 1 shows how the samples from the Zenouz kaolin mine are divided into six subgroups based on physical and chemical characteristics.

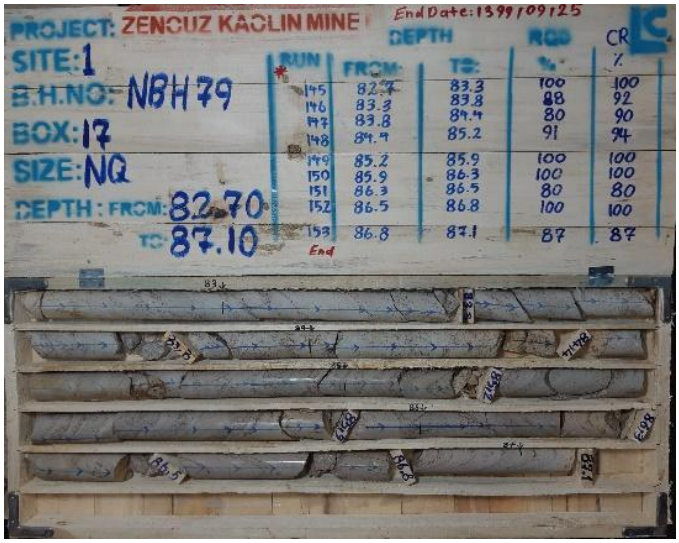

Figure 4. Drilled cores stocking box.

Figure 5. Divided cores which are archived in the box.

Table 1. Characteristics table of kaolin types based on physical and chemical properties.

	Al_2O_3 (%)	Fe_2O_3 (%)	CaO (%)	Whiteness (%)	M.O.R (Kg_f/cm^2)
Type 1	17-20	1-4	3-6	0.0-50	10-20
Type 2	15-17	0.2-0.4	0-0.5	60-100	7-17
Type 3	15-18	0.2-0.5	2-2.5	0-50	0.0
Type 4	15-20	0.2-1.5	2-3	60-75	0-5
Type 5	14-18	0.4-0.8	3-5	70-90	5-15
Type 6	14-18	0.5-1.2	4-6	50-80	5-20

4. Data Collection

Drilled cores that had previously been analyzed and classified based on chemical and physical analyses were used to create and build a reliable and valid labelled dataset. Then, images of these cores were taken in identical circumstances, with the same brightness and distance between the camera and the samples. For each of the six kaolin types, images with a resolution of 666×500 pixels were chosen (see Figure 6).

Figure 6. Taken image of kaolin sample.

Sixty percent of the images were used for learning, and the rest were used for validating. Table 2 indicates the number of images taken for each kaolin type.

Table 2. Number of images dedicated to training and validation.

Kaolin types	Total images' count	Selected images	
		Training	Validation
Type 1	**100**	**60**	**40**
Type 2	**120**	**72**	**48**
Type 3	**80**	**48**	**32**
Type 4	**80**	**48**	**32**
Type 5	**120**	**72**	**48**
Type 6	**110**	**66**	**44**

The images were then organized into related folders based on their categories. Figure 7 shows some instances of various image categories.

5. Dataset Preprocessing

Two preprocessing techniques described below were employed to train the model with the highest accuracy.

5.1. Rescaling

The original images include RGB variables in the band of 0-255, but such values are too large for models to comprehend; therefore, rescaling converts selected values between 0 and 1 rather than the previously indicated range by downsizing through the use of a 1/255 ratio.

5.2. Data Generating

The data generator method is used to resize, rotate, and zoom in on images to prevent our data from overfitting.

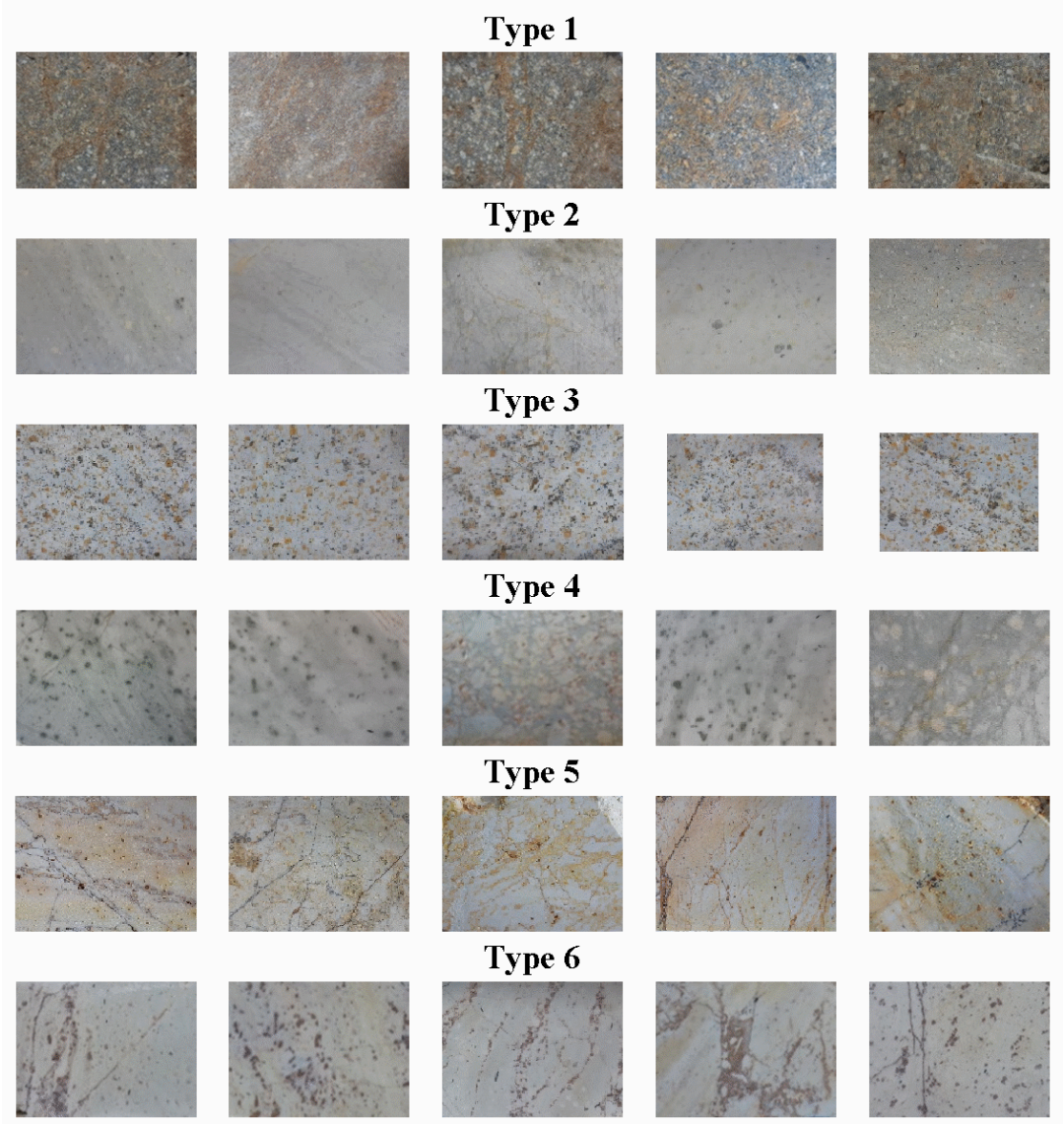

Figure 7. Images of Kaolin samples that have been classified.

6. Model Generation

An eight-layer CNN topology was proposed to recognize the type of kaolin samples. The input images were reduced in size from 666×500 pixels to 100×100 pixels to understand the model better and decrease computing volume. Convolutional layers are typically limited to 5 layers; however,

extra layers were designed in this study to maximize the accuracy of the classification of the samples by taking into account the sample's important and complicated details and the necessity for high precision as two essential factors. After examining various topologies, an eight-layer model was established to determine the sample types. The following are the model's specifications.

The images are input to the model in 100×100×3 shapes meaning the images are 100×100 pixels in size and contain three colours (RGB). The first layer is an (X)×3×3 shape 2D convolutional layer that the first argument controls the number of output channels for the layer (e.g., 16 or 32). In this layer, the same padding is used to ensure the output shape is the same as the input. After the convolutional layer, a max-pooling layer calculates the maximum value for feature map patches. Then, it uses it to produce a new sub-sampled feature with a pool size of 2×2. After that, all the previously specified layers are repeated. In the next phase, the flattened layer is designed to convert 2D feature maps to 1D, and the first dense layer is built to create 64 fully connected neurons. Then, the drop-out layer of 50% is used to reduce overfitting in the network. Finally, the last layer is a dense layer with six neurons that recognize six different types of kaolin samples. Figure 8 shows an eight-layer CNN model created to recognize samples types.

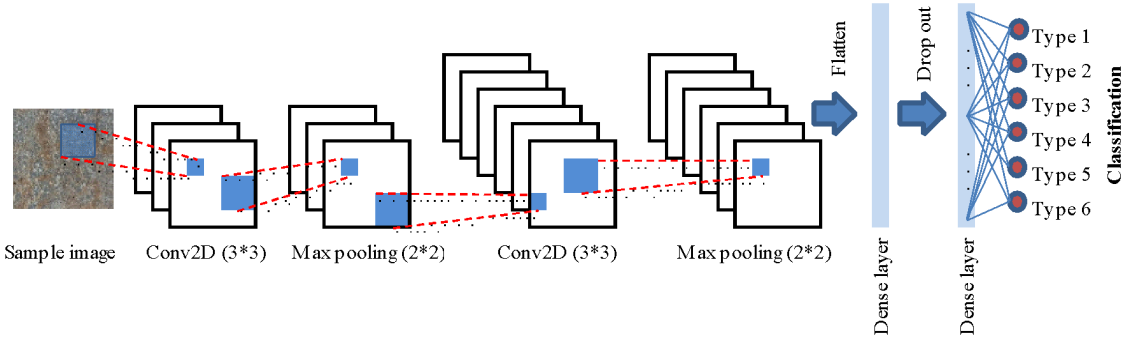

Figure 8. Structure of eight layers CNN model.

Eventually, the model detected sample types based on their related folders and performed training data with 400 steps per batch size and validation data with 200 steps per batch size. Because the accuracy had achieved a fixed state after 200 epochs, the model was completed in 200 epochs to avoid wasting time and expanding the volume of calculations. This paper used two sequential topologies with different features, and the output information was compared. Figure 10 depicts the flowchart of model A and B performances.

7. Model validation

Following a comparison of structures A and B, model A was identified as the most efficient model for training and recognizing sample types, with 90% accuracy versus 84% for model B. Figure 9 compares the accuracy trends of the two models through 200 epochs. Also, the training and validation accuracy trend related to model A is shown in Figure 11.

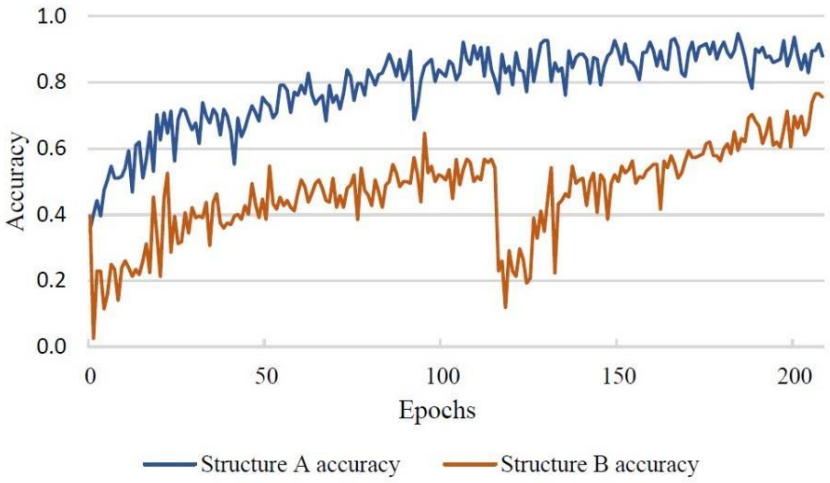

Figure 9. Structures A and B Accuracy.

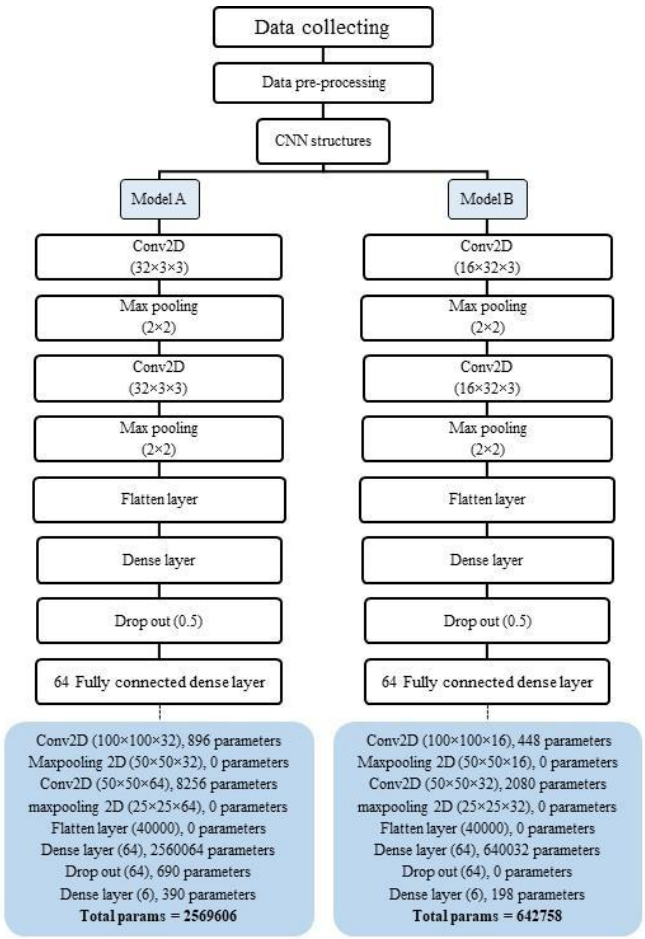

Figure 10. Structure A and B topologies.

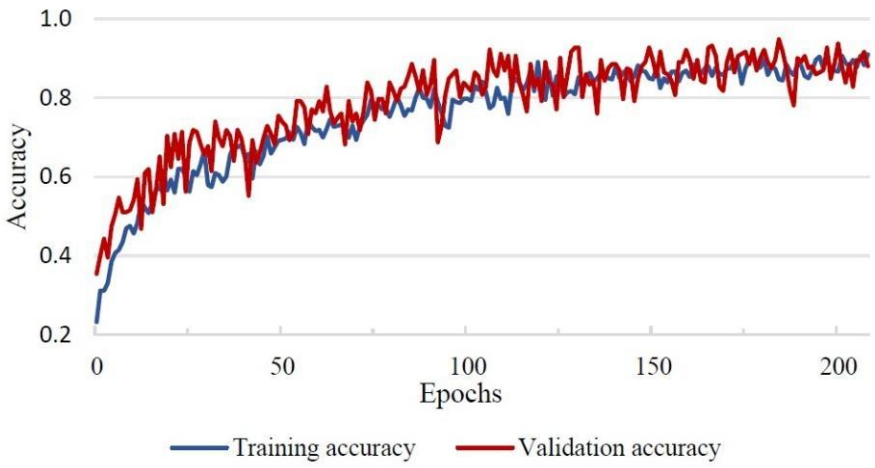

Figure 11. Model A training and validation accuracy trend.

In order to validate the selected model and measure its efficiency, there are unique methods that are described below.

7.1. Accuracy

The accuracy metric is technically expressed as the ratio of accurate classification generated by the model and is formally defined as:

$$Accuracy = \frac{Number\ of\ correct\ predictions}{Total\ number\ of\ predictions} \quad (1)$$

7.2. Precision

The precision for a category in a classification model is the number of true positives divided by the total number of elements labelled as belonging to the positive class.

$$Precision = \frac{True\ possitive}{True\ possitive + False\ possitive} \quad (2)$$

7.3. Recall

In this respect, recall is defined as the number of true positives divided by the total number of components that actually belong to the positive class.

$$Recall = \frac{True\ possitive}{True\ possitive + False\ negative} \quad (3)$$

7.4. F1-score

The F1-score, the harmonic mean of precision and recall, measures a test's accuracy. The F1-score metric can also have a maximum value of 1.0, indicating perfect precision and recall, and a minimum value of 0 if neither precision nor recall is zero.

$$F1 - score = 2 * \frac{Recall * Precision}{Recall + Precision} \quad (4)$$

All four methods were applied in this paper to comprehend the model's reliability better. Table 3 demonstrates the model's efficiency based on each technique for every type.

Table 3. CNN validation metrics.

	Metrics		
Kaolin types	Precision	Recall	F1-score
Type 1	0.85	1.00	0.92
Type 2	0.92	0.92	0.92
Type 3	0.88	0.96	0.92
Type 4	1.00	0.84	0.92
Type 5	0.88	0.96	0.92
Type 6	0.93	0.84	0.88
Total accuracy		0.91	

8. Conclusion

DL has made considerable advances in a spectrum of uses in current history. DL obviously uses automatically detecting characteristics and patterns from inputs mixed with modelling frameworks capable of capturing very complicated behaviour, unlike other ML approaches. With high accuracy and ability to cope with image data, CNNs are the most widespread platform generally available.

Since classifying the types of drilled cores takes a long time and costs a lot, a novel deep learning-based model was developed. The model was tested in the Zenouz kaolin mine, Iran. This model can learn from images of previously analyzed and categorized drilled cores and quickly recognize new samples. Furthermore, the exactness of the model according to four criteria accuracy, precision, recall, and F1-score is equal to 90%, 92%, 92%, and 90%, respectively, which are acceptable accuracies to identify the type of samples when using this approach on six different types of kaolin.

9. References

[1] Alzubaidi, L., Zhang, J., Humaidi, A. J., Al-Dujaili, A., Duan, Y., Al-Shamma, O., Santamaría, J., Fadhel, M. A., Al-Amidie, M., and Farhan, L. (2021). Review of deep learning: concepts, CNN architectures, challenges, applications, future directions. *Journal of Big Data*, *8*

[2] Baykan, N. A. and Yilmaz, N. (2010). Mineral identification using color spaces and artificial neural networks. *Computers and Geosciences*, *36* 91-97.

[3] Chauhan, S., Rühaak, W., Khan, F., Enzmann, F., Mielke, P., Kersten, M., and Sass, I. (2016). Processing of rock core microtomography images: Using seven different machine learning algorithms. *Computers and Geosciences*, *86* 120-128.

[4] Fang, W., Love, P. E. D., Luo, H., and Ding, L. (2020). Computer vision for behaviour-based safety in construction: A review and future directions. *Advanced Engineering Informatics*, *43* 100980.

[5] Fu, Y. and Aldrich, C. (2020). Deep Learning in Mining and Mineral Processing Operations: A Review. *IFAC-PapersOnLine*, *53* (2), 11920-11925.

[6] Gan, S. Q. and Scholz, C. A. (2013). Extracting paleoclimate signals from sediment laminae: An automated 2-D image processing method. *Computers and Geosciences*, *52* 345-355.

[7] Géron, A. (2017). Hands-On Machine Learning with Scikit-Learn and TensorFlow.

[8] Gu, J., Wang, Z., Kuen, J., Ma, L., Shahroudy, A., Shuai, B., Liu, T., Wang, X., Wang, G., Cai, J., and Chen, T. (2018). Recent advances in convolutional neural networks. *Pattern Recognition*, *77* 354-377.

[9] Keyvani, A. and Strom, K. (2013). A fully-automated image processing technique to improve measurement of suspended particles and flocs by removing out-of-focus objects. *Computers and Geosciences*, *52* 189-198.

[10] Lepistö, L. (2005). Rock image classification using color features in Gabor space. *Journal of Electronic Imaging*, *14* 040503.

[11] Li, H. C., Deng, Z. Y., and Chiang, H. H. (2020). Lightweight and resource-constrained learning network for face recognition with performance optimization. *Sensors (Switzerland)*, *20* 1-20.

[12] Liu, C., Tang, C. S., Shi, B., and Suo, W. B. (2013). Automatic quantification of crack patterns by image processing. *Computers and Geosciences*, *57* 77-80.

[13] Liu, Y., Zhang, Z., Liu, X., Wang, L., and Xia, X. (2021). Deep learning-based image classification for online multi-coal and multi-class sorting. *Computers and Geosciences*, *157* 104922.

[14] Maiti, A., Chakravarty, D., Biswas, K., and Halder, A. (2017). Development of a mass model in estimating weight-wise particle size distribution using digital image processing. *International Journal of Mining Science and Technology*, *27* 435-443.

[15] Maitre, J., Bouchard, K., and Bédard, L. P. (2019). Mineral grains recognition using computer vision and machine learning. *Computers and Geosciences*, *130* 84-93.

[16] Ouanan, H. and Abdelwahed, E. H. (2019). Image processing and machine learning applications in mining industry: Mine 4.0. *Proceedings - 2019 International Conference on Intelligent Systems and Advanced Computing Sciences, ISACS 2019*, 1-5.

[17] Palaz, D., Magimai-Doss, M., and Collobert, R. (2019). End-to-end acoustic modeling using convolutional neural networks for HMM-based automatic speech recognition. *Speech Communication*, *108* 15-32.

[18] Patel, A. K. and Chatterjee, S. (2016). Computer vision-based limestone rock-type classification using probabilistic neural network. *Geoscience Frontiers*, *7* 53-60.

[19] Ramil, A., López, A. J., Pozo-Antonio, J. S., and Rivas, T. (2018). A computer vision system for identification of granite-forming minerals based on RGB data and artificial neural networks. *Measurement: Journal of the International Measurement Confederation*, *117* 90-95.

[20] Ran, X., Xue, L., Zhang, Y., Liu, Z., Sang, X., and He, J. (2019). Rock Classification from Field Image Patches Analyzed Using a Deep Convolutional Neural Network. 1-16.

[21] Safari, H., Balcom, B. J., and Afrough, A. (2021). Characterization of pore and grain size distributions in porous geological samples – An image processing workflow. *Computers and Geosciences*, *156* 104895.

[22] Singh, V. and Mohan Rao, S. (2005). Application of image processing and radial basis neural network techniques for ore sorting and ore classification. *Minerals Engineering*, *18* 1412-1420.

[23] Socher, R., Perelygin, A., Wu, J., Chuang, J., Manning, C. D., Ng, A., and Potts, C. (2013). *Recursive Deep Models for Semantic Compositionality Over a Sentiment Treebank*. in Proceedings of EMNLP.